JOURNAL OF THERMOPHYSICS AND HEAT TRANSFER
Vol. 8, No. 3, July–Sept. 1994

Examination of Theory for Bow Shock Ultraviolet Rocket Experiments—I

Deborah A. Levin*
Institute for Defense Analyses, Alexandria, Virginia 22311
Graham V. Candler†
North Carolina State University, Raleigh, North Carolina 27695
Robert J. Collins‡
University of Minnesota, Minneapolis, Minnesota 55455
Peter W. Erdman§ and Edward C. Zipf¶
University of Pittsburgh, Pittsburgh, Pennsylvania 15260
and
L. Carl Howlett**
Utah State University, Logan, Utah 84322

Comparison is made between the results obtained from modifications to a state-of-the-art radiation code and bow shock uv radiation data obtained from recent flight experiments. Initial predictions of the radiation did not yield satisfactory comparison with the first flight experiment flown at 3.5 km/s between altitudes of 40–70 km, despite improvements to the original flow model. It is found that characterizing the NO excited state population with the translational temperature, rather than the vibrational temperature, yields better comparison to the flight data. Comparison of bow shock data from the second flight, flown at 5.1 km/s at altitudes of 70–90 km, shows that improvements in either flow or radiation modeling are still needed, particularly at high altitudes.

Introduction

THE first bow shock flight experiment (April 1990) measured the uv radiation from shock-heated gas in the nose region of a 0.1016-m nose radius rocket traveling at 3.5 km/s at altitudes from 40 to 70 km. Two recent papers discussed the instruments and results[1] obtained from the flight and analyses of that data.[2] The calculations undertaken in Ref. 2 attempted to improve the predictive capabilities above 50 km. The flow model that was originally used[3] was augmented to include wall-slip effects, an approximate nonlinear constitutive relation, and rotational nonequilibrium. Solutions obtained with the enhanced flowfield model and the NEQAIR[4] radiation model did not appreciably improve the radiation predictions, which were in error by many orders of magnitude at altitudes of 50 km and higher. (See Fig. 1 and compare "baseline" model to the data.)

Recent shock tube studies[5] suggested an alternative way to compute the effective electronic excitation temperature for NO gamma and beta band emission in the NEQAIR model. This article will discuss that change and show comparison with flight data. The second theory article,[6] will discuss our analyses of the NEQAIR model for the flow conditions of the Bow Shock 1 and 2 flight experiments.

A second flight experiment, flown February 1991, obtained data during re-entry for a speed of 5.1 km/s at altitudes from 90 to 70 km. Papers providing details on the instrumentation and results[7] and analyses[8] of the rearward plume measurements have been presented. In this article the postulated changes to the NEQAIR radiation model are compared with re-entry data from the second flight. A companion article will discuss the instrumentation used and data obtained during re-entry for the second flight.[9]

In contrast to the first flight predictions, computed second flight radiances do not show the same altitude dependence as the UV data. This lack of agreement can be caused by inadequate NO chemistry in the flow modeling. Variation of the O_2 dissociation rate was examined, as it is the rate controlling step in the production of NO.

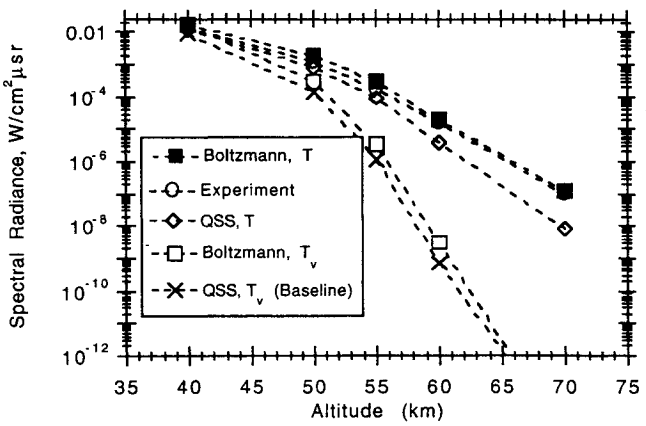

Fig. 1 Comparison of radiation models with Bow Shock 1 flight data; 230-nm, 0-deg viewing geometry.

Presented as Paper 92-2871 at the AIAA 27th Thermophysics Conference, Nashville, TN, July 6–8, 1992; received June 16, 1993; revision received Oct. 5, 1993; accepted for publication Oct. 6, 1993.

*Research Staff Member, Science and Technology Division. Member AIAA.
†Assistant Professor, Department of Mechanical and Aerospace Engineering. Member AIAA.
‡Professor, Department of Electrical Engineering.
§Research Associate Professor, Department of Physics and Astronomy. Member AIAA.
¶Professor, Department of Physics and Astronomy. Member AIAA.
**Technical Program Manager, Center for Space Engineering. Member AIAA.

The increase in velocity compared to that of the first flight (3.5 km/s) offers an opportunity to validate the models at higher temperatures. Gas temperatures from the first flight are about 5000 K, whereas flow modeling of the second flight produces translational temperatures close to 14,000 K. The difference in altitude for which data were obtained is also an important factor. Data were obtained for the first flight between altitudes of 40–70 km for most of the instruments. The second flight tests the rarefaction and nonequilibrium aspects of the flow and radiation modeling at higher altitudes.

Off-axis 230-nm photometer data from the second flight permits two-dimensional comparison of the flow and radiation modeling. The analysis of this data was complicated by rocket precession. Reference 9 discusses the signal modulation correlation with the angle from the instantaneous stagnation point. The modeling predictions are compared with corrected off-axis data for a continuous set of angles of 15–45 deg from the rocket longitudinal axis.

Flowfield Simulation Method

The computational fluid dynamics technique that is used to simulate the stagnation region along the experimental trajectory is discussed in Ref. 2. However, some changes have been made to the thermophysical model for air, and therefore, it is described here.

The model for air is a reacting mixture of perfect gases composed of eight chemical species (N_2, O_2, NO, NO^+, N_2^+, N, O, and e^-). These species are allowed to react with one another at finite rates. The internal energy is described by translational, rotational, and vibrational-electron temperatures. Finite-rate relaxation of the rotational and vibrational temperatures to the translational temperature is modeled. To simulate a gas with this chemical model, we must solve a separate mass conservation equation for each chemical species and a separate energy equation for each energy mode. The rotational energy per unit volume is given by

$$E_r = \sum_{s=\text{dia}} \rho_s e_{rs} = \sum_{s=\text{dia}} \rho_s \frac{R}{M_s} T_r \tag{1}$$

where the summation index s is over diatomic molecules. The vibrational-electron-electronic energy may be related to the vibrational temperature using a simple harmonic oscillator model and the first two excited electronic states[10]

$$E_v = \sum_{s=\text{dia}} \rho_s e_{vs} + \sum_{s\neq e} \rho_s e_{els} + \rho_e e_e \tag{2}$$

The total energy is given by

$$E = \sum_{\substack{s\neq e \\ 0}} \rho_s \frac{3}{2}\frac{R}{M_s} + E_r + E_v + \frac{1}{2}\rho(u^2 + v^2) + \sum_s \rho_s h_s^0 \tag{3}$$

where h_s is the heat of formation.

The rate of energy transfer from translation to rotation is given by

$$Q_{T-R} = \sum_{s=\text{dia}} \left[\rho_s \frac{e_{rs}^*(T) - e_{rs}}{\langle \tau_{rs} \rangle} + w_s e_{rs} \right] \tag{4}$$

The second term in Eq. (4) results from conservation of rotational energy during chemical reactions. The rotational relaxation time $\langle \tau_{rs} \rangle$ is obtained from the work of Lordi and Mates,[11] wherein they use the work of Parker[12] to obtain the following expression for the rotational relaxation time of species s by species t:

$$\tau_{rst} = \tau_{cst} \frac{Z_{Rs}^\infty}{1 + \frac{\pi^{3/2}}{2}\sqrt{T_s^*/T} + \left(\frac{\pi^2}{4} + \pi\right) T_s^*/T} \tag{5}$$

where τ_{cst} is the collision time between particles s and t. The average relaxation time $\langle \tau_{rs} \rangle$ is found by number-weighting the individual relaxation times. The constants used in the Parker model and the collision diameters are given in Table 1 for the primary species used in this work.

The rate of energy transfer from translation to vibration Q_{T-V} is based on the Landau-Teller model for harmonic oscillators.[10] We can write this as

$$Q_{T-V} = \sum_{s=\text{dia}} \left[\rho_s \frac{e_{vs}^*(T) - e_{vs}}{\langle \tau_{vs} \rangle} + w_s e_{vs} \right] \tag{6}$$

where e_{vs} and $e_{vs}^*(T)$ are the vibrational energy per mass contained in a simple harmonic oscillator at the local vibrational and translational temperatures, respectively. $\langle \tau_{vs} \rangle$ is the average vibrational relaxation time of species s, and is obtained by number-weighting the individual vibrational relaxation times from the interaction of s with itself and the other chemical species. These relaxation times are obtained from the semi-empirical expression from Millikan and White.[13] However, as discussed in Ref. 2, an effort has been made to improve the relaxation times for specific interactions using more recent data than were available to Millikan and White. The appropriate parameters are summarized in Ref. 2. Additionally, the collision-limiting concept discussed by Park[14] is used to prevent the relaxation time from becoming artificially small at high temperatures.

For the eight-species air model, eight reactions are considered

$$\begin{aligned}
N_2 + M &\leftrightarrows N + N + M \\
O_2 + M &\leftrightarrows O + O + M \\
NO + M &\leftrightarrows N + O + M \\
N_2 + O &\leftrightarrows NO + N \\
NO + O &\leftrightarrows O_2 + N \\
N + O &\leftrightarrows NO^+ + e- \\
N + N &\leftrightarrows N_2^+ + e- \\
NO^+ + N &\leftrightarrows N_2^+ + O
\end{aligned} \tag{7}$$

The chemical reaction rates are obtained from Park.[15] It is assumed that for situations where there is vibrational nonequilibrium, i.e., where $T \neq T_v$, the dissociation reactions are governed by the geometric average of these two temperatures, $\sqrt{TT_v}$. This yields a more realistic dissociation rate in regions where the flow is in thermal nonequilibrium.[14]

The governing equations described by this model are solved using a Gauss-Seidel line relaxation method proposed by MacCormack.[16] Modified Steger-Warming flux-vector splitting[17] is used for the spatial differencing.

The computational technique was used to simulate the stagnation region flowfield at points along the trajectories of the two flights. The chemical species concentrations and temperatures obtained from the flowfield simulation are used in NEQAIR[4] (non equilibrium air radiation) to compute the radiation in the uv spectral region. It is assumed that the flow is optically thin and that radiative heat losses from the gas can be neglected. It is further assumed that the excited electronic states are populated according to the vibrational temperature T_v, but that this distribution is a quasi-steady-state

Table 1 Molecular constants for the use in the rotational relaxation model

Species	Z_{Rs}^∞	T_s^*, K	d_s, Å
N_2	23	91.50	3.709
O_2	23	113.00	3.608
NO	23	102.25	3.534

(QSS) distribution. The flow model used in this manner has been shown to give good agreement with flight data taken at higher speeds than the present experiments.[14]

The purpose of this article is to test some of the above assumptions, particularly with regard to the interpretation of the roles of T and T_v. It will be seen that the re-interpretation of the translational temperature as the temperature that governs the population of the NO excited states improves the comparison to flight data for both flights.

Changes to the Radiation Model and Application to the First Flight Conditions

The NEQAIR radiation model, as originally developed by Park,[4] uses the species concentrations and temperatures calculated from the flowfield to determine an effective electronic excitation temperature $T_{\text{eff},i}^e$ for the ith electronic state. The model for the NO molecule includes the first two electronic levels, $A^2\Sigma^+$ and $B^2\Pi^+$; although, more recent versions of the model now incorporate the $C^2\Pi$ and $D^2\Sigma^+$ higher lying electronic levels.[18] The conclusions drawn in this article are not altered by the lack of these additional electronic states, since comparison with data is restricted to the 230-nm photometers, a spectral region not significantly affected by the C and D state contributions. For more detailed comparison with spectral data, the inclusion of the D state should be considered.[18] The radiation modeling assumes that there are a sufficient number of collisions to define an electronic excitation temperature, but that there are not enough to establish a Boltzmann distribution. Also, the rates of population and depopulation of the electronic excited states are assumed to be much faster than the overall change in these levels; i.e., the excitation and de-excitation rates nearly balance each other. Under these conditions, a QSS distribution exists. Therefore, the electronic excitation temperature is dependent on various excitation and de-excitation cross sections and radiative transition rates (which will be discussed in Ref. 6). It is also dependent on the choice of governing temperature T_{gov} that is assumed to characterize the distribution of excited electronic states. The baseline version of NEQAIR assumes T_{gov} is T_v.

To test the sensitivity of the calculations to the assumptions made in modeling the radiation, results were obtained for the baseline and three alternative models. The four models use either a Boltzmann distribution or a QSS distribution of the excited electronic states, each of which may be governed by either the translational or vibrational temperature. Table 2 summarizes the differences between the models used in the simulations. Figure 1 shows these results compared to the radiation from the 230 nm, 0-deg viewing photometer for the first flight. The baseline NEQAIR approach yields poor agreement with the experiment for altitudes above 50 km. The top curve shows results of radiation calculations based on a Boltzmann distribution of the NO excited states governed by the local translational temperature and the NO concentration. This assumption brings the theory into better agreement with experiment; however, this approach overpredicts the radiation at altitudes lower than 60 km. Calculations were also made assuming a Boltzmann distribution with T_v as the governing temperature. The results are essentially the same as the baseline model. A comparison of these results shows that the choice of the temperature that characterizes the electronic state distribution is more critical than assumptions regarding the thermal degree of equilibration. Therefore, it would appear that the governing temperature for NO excited state population is the heavy particle translational temperature.

Table 2 Radiation models used in the computation of NO radiation

Model	NO excited state distribution	T_{gov}
Baseline	QSS	T_v
Boltzmann, T_v	Boltzmann	T_v
QSS, T	QSS	T
Boltzmann, T	Boltzmann	T

A more plausible description of the excited state population than the Boltzmann distribution is a QSS distribution governed by the translational temperature. This differs from the baseline NEQAIR model in that all rates for excitation of electronic states by collisions with neutrals are calculated with T, rather than T_v. T_v continues to be used to represent the distribution of vibrational states for a given electronic state in the calculation of the molecular partition functions. The results obtained with this approach are plotted in Fig. 1. These results show good agreement with experiment; however, for 55 km and higher, they fall below the experiment. Figure 2 shows a similar comparison of the radiation models and the 230-nm, 30-deg viewing photometer data. The results are similar, with the experiment falling between the results of the QSS and Boltzmann distributions governed by the translational temperature. To complete the set, Fig. 3 shows the same comparisons for the 230-nm, 50-deg viewing photometer.

The predictions using T_v as the governing temperature have a different altitude dependence than the other simulations or the data. However, the results obtained using models based on the translational temperature have an altitude variation similar to the data. Therefore, the translational temperature appears to govern the excited state population of the NO molecules under these flight conditions. Reference 18 also shows good agreement between spectra computed with the QSS-T model and spectral data over a wide range of altitudes.

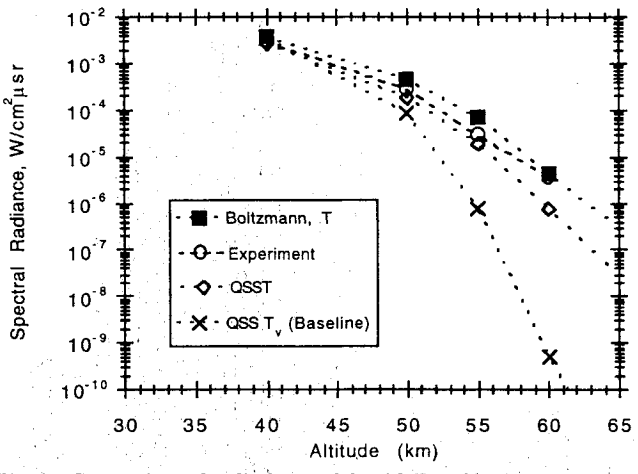

Fig. 2 Comparison of radiation models with Bow Shock 1 flight data; 230-nm, 30-deg viewing geometry.

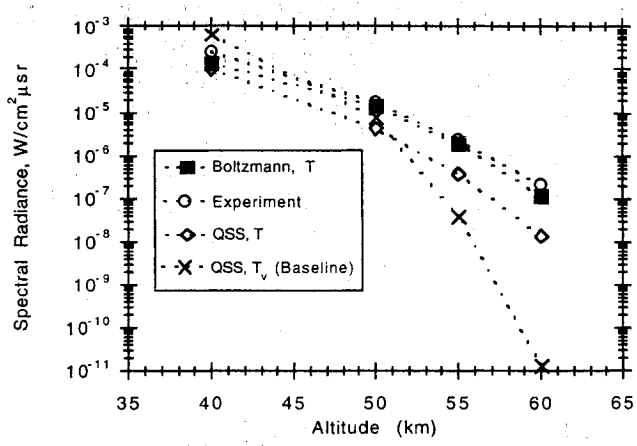

Fig. 3 Comparison of radiation models with Bow Shock 1 flight data; 230-nm, 50-deg viewing geometry.

Application to the Second Flight Conditions—0-Deg Viewing

Figure 4 shows the results of the three radiation models described above applied to the conditions of the second flight and the forward-viewing 230-nm photometer data. The altitude region for which there was sufficient signal to noise and nominal instrument response is between 67–86 km. Figure 13 of Ref. 9 shows the consistency of the photometer data with independent spectroscopic measurements. The computations are shown in Fig. 4 for altitudes between 55–87 km.

A number of important features are evident from the figure. The results from the three models approach one another at lower altitudes where the flow approaches equilibrium. At higher altitudes the computational results diverge from one another, with the model based on the QSS distribution governed by the translational temperature approximately following the experimental results. Thus, the calculations again show that the translational temperature, rather than the vibrational temperature, continues to be more representative of the electronic excitation temperature of the NO molecule. However, unlike the comparisons to the first flight, the data show a different altitude dependence than the computations, falling off more slowly with altitude. None of the present models fit the entire altitude range for which data were obtained during the second flight.

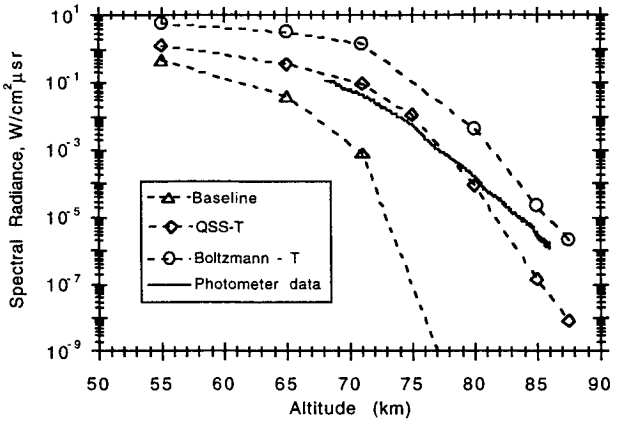

Fig. 4 Comparison of radiation models with Bow Shock 2 flight data; 230-nm, 0-deg viewing photometer.

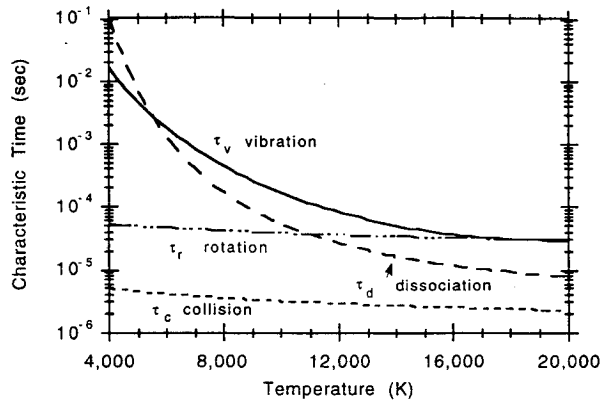

Fig. 5 Comparison of O_2 relaxation, dissociation, and collision times at a typical density ($\rho = 1.0 \times 10^{-4}$ kg/m³).

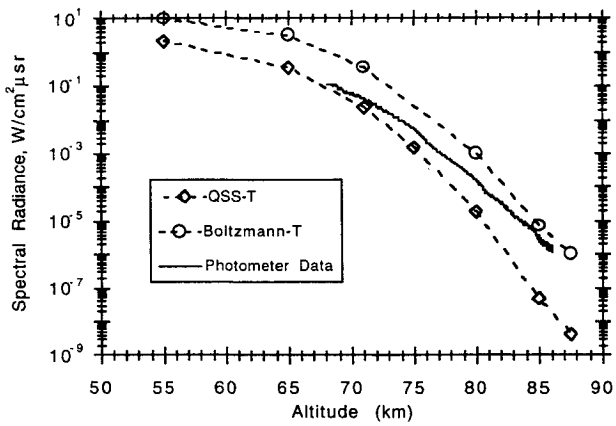

Fig. 6 Effect of Wray[18] O_2 dissociation rate on comparison of radiation models with Bow Shock 2 flight data; 230-nm, 0-deg viewing photometer.

The inability of theory to predict the observed radiance dependence on altitude may be caused by either remaining inadequacies in the radiation model[6] or prediction of the amount of NO produced in the flowfield. In these conditions, the production of NO is primarily limited by the rate of production of O through the dissociation of O_2. The O_2 dissociation time is plotted against the rotational and vibrational relaxation times of the O_2 molecule in Fig. 5 for a typical density ($\rho = 1.0 \times 10^{-4}$ kg/m³). We have defined the dissociation time as

$$\tau_d = (\bar{M}/\rho k_d) \tag{8}$$

where k_d is the dissociation rate and $\bar{M}$ is the average molecular weight. It is clear from this figure that the dissociation time becomes aphysically small at high temperatures, being less than the vibrational relaxation time above 5500 K, and less than the rotational relaxation time above 11,000 K. Wray[19] measured dissociation of O_2 by the Argon atom at temperatures similar to those of the second flight. The dissociation rate used in the calculations was obtained from Wray's dissociation rate of O_2 by Ar. This rate was multiplied by a catalytic efficiency of 9 for molecules and 25 for atoms. However, Wray analyzed the catalytic efficiency at temperatures similar to those in the second flight (10,000–14,000 K). He found that the catalytic efficiency of oxygen atoms relative to Argon is no more than 1.3 at high temperatures. Thus, it appears that using a lower catalytic efficiency for the second flight condition is warranted. The flowfields were recomputed using catalytic efficiencies of unity for all of the third-bodies in the O_2 dissociation rate. The radiation produced by these flowfields are presented in Fig. 6. Here we see that the data now fall between the two radiation models governed by the translational temperature. The decrease in the radiation is almost entirely due to the decrease in the number of NO molecules. However, with both dissociation models, the comparison at high altitudes is poor, indicating another source of error in the modeling.

Comparison of First and Second Flight Regimes

There are several differences between the first and second flight that make the second flight conditions a more stringent test of the modeling. The difficulties in the flow modeling are associated with the rarefied nature of these flows and the resulting uncertainties in the temperatures and species concentrations. The radiation modeling is uncertain due to errors in excitation cross sections and the temperature and accuracy of the QSS approximation.

Assessment of the accuracy of the modeling of temperatures and species concentrations in a more rarefied flow regime than studied before is crucial. Temperatures for Bow Shock 1 were about 5000 K. Thermal nonequilibrium in the flow produced differences between the vibrational and translational temperatures of about 1000 K. The translational and rotational temperatures were essentially equilibrated.[2] Figure 7 shows an example of temperatures obtained from the flow model for one of the second flight trajectory points at 80 km and 5.1 km/s. The degree of nonequilibrium can be seen to be much greater than observed for the first flight. Figures 8 and 9 show a comparison of the calculated NO stagnation streamline concentrations for first and second flight conditions, respectively. In Ref. 2 we showed that the kinetics for

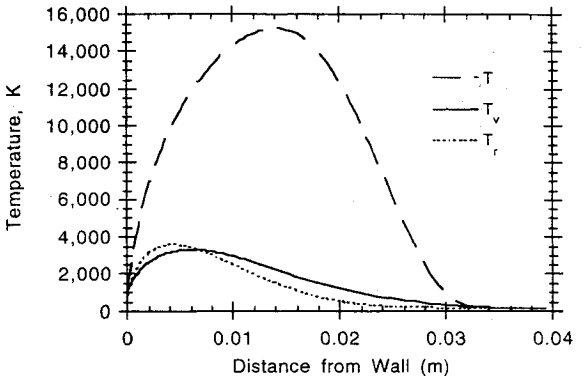

Fig. 7 Stagnation streamline calculated temperatures for Bow Shock 2 experiment conditions of 80 km and 5.1 km/s.

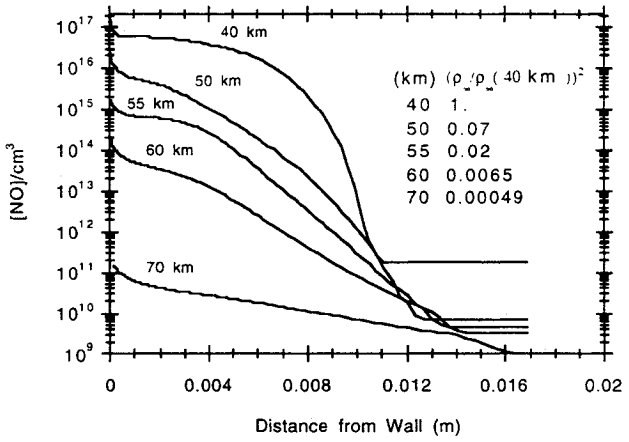

Fig. 8 Comparison of NO stagnation streamline concentrations for the Bow Shock 1 flight regime with freestream density scaling.

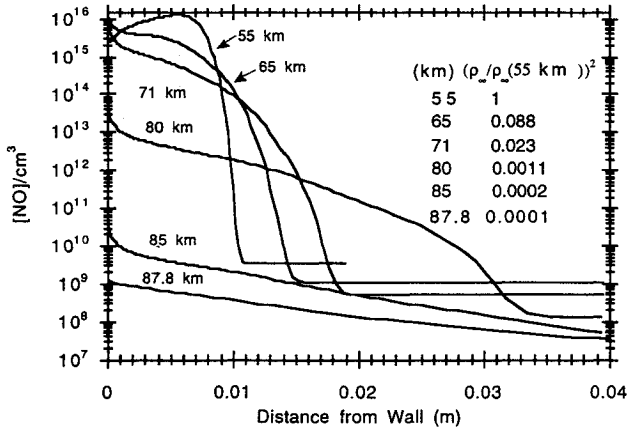

Fig. 9 Comparison of NO stagnation streamline concentrations for the Bow Shock 2 flight regime with freestream density scaling.

formation of NO is second-order in freestream density. The figures also show a tabulation of the square of the freestream density normalized to the lowest altitude case modeled. The tabulation provides an interesting comparison with the calculated NO concentrations in the vicinity of the wall. At altitudes greater than about 80 km the drop in density ratios is greater for the second flight than the first. The calculated NO wall densities at different trajectory conditions in Fig. 8 scale as the freestream density ratios for the first flight conditions, except at the highest altitude of 70 km. Figure 9 shows that the agreement between calculated wall density ratios deviates significantly from the freestream scaling for the second flight conditions. The high degree of rarefaction for the second flight conditions suggest that rarefaction corrections employed in the flow modeling may be inadequate. Future comparisons

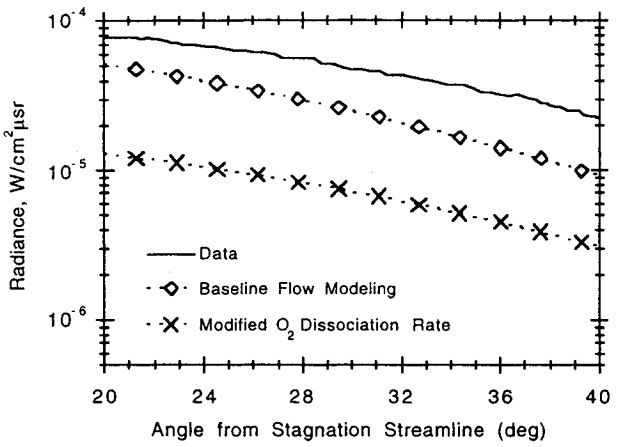

Fig. 10 Comparison of off-axis 230-nm photometer data from the second bow shock flight experiment with calculations at TALO of 347 s, ~80 km.

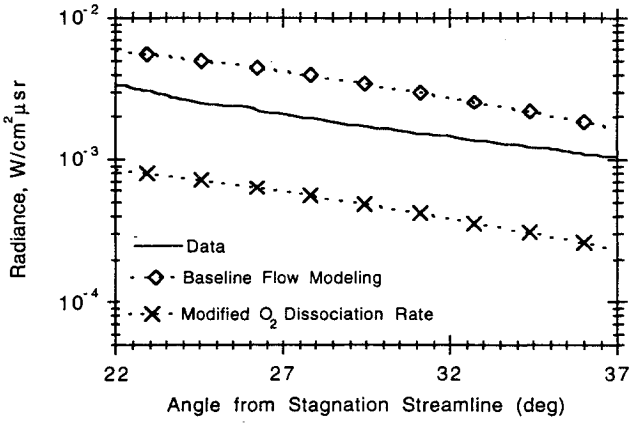

Fig. 11 Comparison of off-axis 230-nm photometer data from the second bow shock flight experiment with calculations at TALO of 355 s, ~75 km.

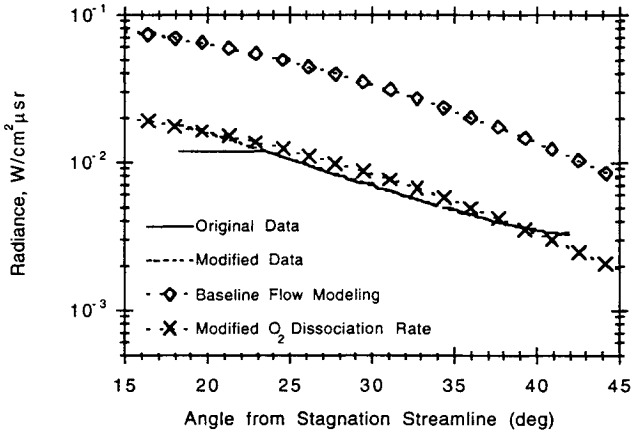

Fig. 12 Comparison of off-axis 230-nm photometer data from the second bow shock flight experiment with calculations at TALO of 358 s, ~73 km. Saturation effects at small angles can be seen in the original data. The curve labeled modified data has removed saturation by peak interpolation.

with direct simulation Monte Carlo calculations may help assess this uncertainty.[20]

Application to the Second Flight Conditions—Off-Axis

The second flight also provided instrumentation for viewing the flow at angles of 30 and 50 deg from the rocket longitudinal axis. As mentioned in the companion experimental article,[9] the nonoptimum separation of the second and third stages induced a precessional motion upon re-entry. As a result, the

30- and 50-deg photometers viewed the flow at angles from about 20–60 deg. In Ref. 9 the precession motion was analyzed and it was shown that the "instantaneous" angle from the stagnation streamline could be correlated with time, and hence, altitude. Therefore, we obtained detailed off-axis radiance measurements. The following results illustrate the level of agreement with theory and off-axis data. The comparison emphasizes the angular dependence, as it has already been shown that the theory cannot satisfactorily reproduce the absolute magnitude. The portions of the data chosen were time periods *after* adequate signal-to-noise was obtained, and *before* instrument saturation occurred.

Figures 10–12 show comparisons between data and calculations for altitudes at 80, 75, and 73 km, respectively. The data are taken from the 230-nm 30-deg viewing photometer. When the 30- and 50-deg 230-nm photometers were compared at angles where the data sets overlap, they were found to agree within about 50%. The calculations (each computed at a fixed altitude) in all three figures show a similar angular dependence to the data. This validates the off-axis simulation of the flowfield. The reduction in signal with increasing angle is due to the lower temperature behind the oblique shock, which reduces the production of NO molecules. Also, as the gas that encounters the vehicle near the stagnation point is swept around the body, it expands and reduces its temperature. The comparisons suggest that for larger angles, or less dense flows, the modeling underpredicts the data. However, the comparison of data and theory shown in Fig. 12 may be complicated by data saturation.

Conclusions

A computational fluid dynamics method and a radiation model have been used to simulate the radiation from two flight experiments. These results show that the temperature that governs the NO excited states is the translational temperature, rather than the vibrational temperature. Good agreement between the computations and the experimental 230-nm photometer data were obtained for the first flight, flown at 3.5 km/s. The same radiation model did not give the observed altitude variation of radiance at the second flight conditions 5.1 km/s, although the baseline theory was clearly shown to be incorrect. It appears that there is some question about the applicability of the current O_2 dissociation model at the high temperatures encountered during the second flight. The temperatures, degree of rarefaction, and the amount of nonequilibrium are different for the second flight than the first. Work is ongoing to examine the modeling of these aspects to determine its adequacy at the second flight conditions. The detailed comparison of off-axis experiment and theory for the second flight show good agreement; however, at larger angles, or less dense flow, the theory underpredicts the data. The upcoming article[6] examines the radiation model with respect to the validity of key assumptions used to predict radiation in the 230-nm spectral region.

References

[1]Erdman, P., Zipf, E., Espy, P., Howlett, C., Loda, R., Collins, R., Levin, D., and Candler, G., "Flight Measurements of Low Velocity Bow Shock Ultraviolet Radiation," *Journal of Thermophysics and Heat Transfer*, Vol. 7, No. 1, 1993, pp. 37–41.

[2]Levin, D., Candler, G., Collins, R., Erdman, P., Zipf, E., Espy, P., and Howlett, C., "Comparison of Theory with Experiment for the Bow Shock Ultraviolet Rocket Flight," *Journal of Thermophysics and Heat Transfer*, Vol. 7, No. 1, 1993, pp. 30–36.

[3]Levin, D., Collins, R., and Candler, G., "Computations for Support Design of Measurements of Radiation from Low Velocity Shock Heated Air," *Journal of Thermophysics and Heat Transfer*, Vol. 5, 1991, pp. 463–468.

[4]Park, C., "Calculation of Nonequilibrium Radiation in the Flight Regimes of Aero-Assisted Orbital Transfer Vehicles," *Thermal Design of Aero-Assisted Orbital Transfer Vehicles*, edited by H. F. Nelson, Vol. 96, Progress in Astronautics and Aeronautics, AIAA, New York, 1985.

[5]Meier, U. E., Raiche, G. A., Crosley, D. R., Smith, G. P., and Eckstrom, D. J., "Laser-Induced Fluorescence Decay Lifetimes of Shock-Heated NO(A)," *Applied Physics. B.*, Vol. 53, 1991, pp. 138–141.

[6]Levin, D., Braunstein, M., Candler, G., Collins, R., and Smith, G., "Examination of Theory for Bow Shock Ultraviolet Rocket Experiments—II," *Journal of Thermophysics and Heat Transfer*, Vol. 8, No. 3, 1994, pp. 453–459.

[7]Erdman, P., Zipf, E., Espy, P., Howlett, C., Christou, C., Levin, D., Collins, R., and Candler, G., "In-Situ Measurements of UV and VUV Radiation from a Rocket Plume and Re-Entry Bow Shock," *Journal of Thermophysics and Heat Transfer* (to be published).

[8]Candler, G., Levin, D., Brandenburg, J., Collins, R., Erdman, P., Zipf, E., and Howlett, C., "Comparison of Theory with Plume Radiance Measurements from the Bow Shock Ultraviolet 2 Rocket Flight," *Journal of Thermophysics and Heat Transfer* (to be published).

[9]Erdman, P., Zipf, E., Howlett, C., Levin, D., Collins, R., and Candler, G., "Measurements of Ultraviolet Radiation from a 5 km/s Bow Shock," *Journal of Thermophysics and Heat Transfer*, Vol. 8, No. 3, 1994, pp. 441–446.

[10]Vincenti, W. G., and Kruger, C. H., Jr., *Introduction to Physical Gas Dynamics*, Krieger Publishing, FL, 1965.

[11]Lordi, J. A., and Mates, R. E., "Rotational Relaxation in Nonpolar Diatomic Gases," *Physics of Fluids*, Vol. 13, No. 2, 1970, pp. 291–308.

[12]Parker, J. G., "Rotational and Vibrational Relaxation in Diatomic Gases," *Physics of Fluids*, Vol. 2, No. 4, 1959, pp. 449–462.

[13]Millikan, R. C., and White, D. R., "Systematics of Vibrational Relaxation," *Journal of Chemical Physics*, Vol. 39, No. 12, 1963, pp. 3209–3213.

[14]Park, C., "Assessment of Two-Temperature Kinetic Model for Ionizing Air," AIAA Paper 87-1574, June 1987.

[15]Park, C., "On Convergence of Computation of Chemically Reacting Flows," AIAA Paper 85-0247, Jan. 1985.

[16]MacCormack, R. W., "Current Status of the Numerical Solutions of the Navier-Stokes Equations," AIAA Paper 85-0032, Jan. 1985.

[17]MacCormack, R. W., and Candler, G. V., "The Solution of the Navier-Stokes Equations Using Gauss-Seidel Line Relaxation," *Computers and Fluids*, Vol. 17, No. 1, 1989, pp. 135–150.

[18]Moreau, S., Laux, C., Chapman, D., and MacCormack R., "A More Accurate Nonequilibrium Air Radiation Code:NEQAIR Second Generation," AIAA Paper 92-2968, July 1992.

[19]Wray, K. L., "Shock-Tube Study of the Coupling of the O_2-Ar Rates of Dissociation and Vibrational Relaxation," *Journal of Chemical Physics*, Vol. 37, No. 4, 1962, pp. 1254–1263.

[20]Candler, G., Boyd, I., Levin, D., Moreau, S., and Erdman, P., "Continuum and DSMC Analysis of Bow Shock Flight Experiments," AIAA Paper 93-0275, Jan. 1993.